Surface stabilization of formamidinium perovskite solar cell using quaternary ammonium salt

*Sungwon Song†, Seok Joo Yang†, Jinhyeok Choi, Se Gyo Han, Kwanghee Park, Hansol Lee, Jiwoo Min, Sunmin Ryu and Kilwon Cho**

S. Song, S. J. Yang, J. Choi, S. G. Han, J. Min, H. Lee and Prof. K. Cho

Department of Chemical Engineering, Pohang University of Science and Technology, Pohang, 37673, Korea
E-mail: kwcho@postech.ac.kr

K. Park and Prof. S. Ryu

Department of Chemistry, Pohang University of Science and Technology, Pohang, 37673, Korea

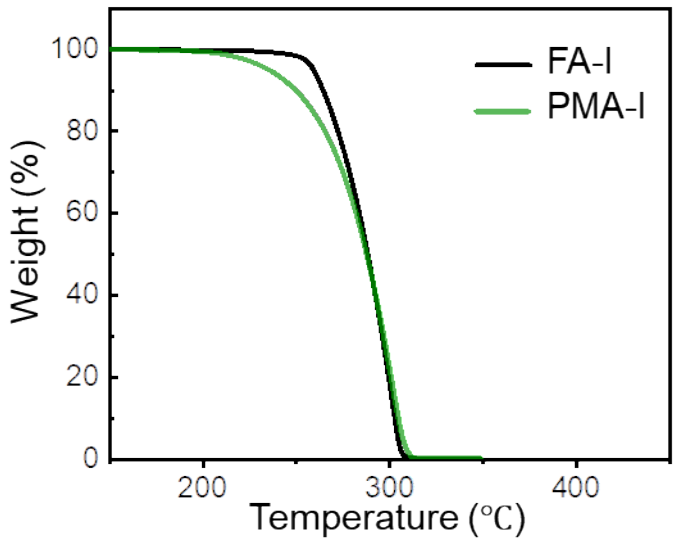

Figure S1. TGA thermograms of FA-I and PMA-I. The decomposition onset temperature of FA-I is 271.4 ℃ which is higher than that of PMA-I. The resonance structure of FA ion makes it less acidic than PMA ion.

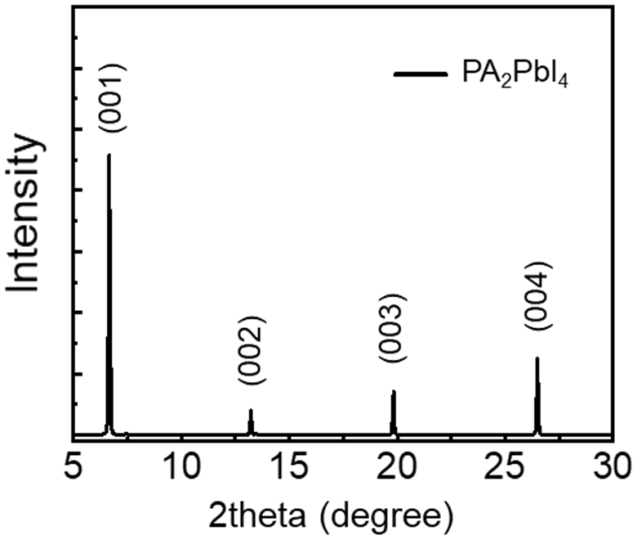

Figure S2. XRD pattern of of PA_2PbI_4 heated at T= 60℃ for 30sec.

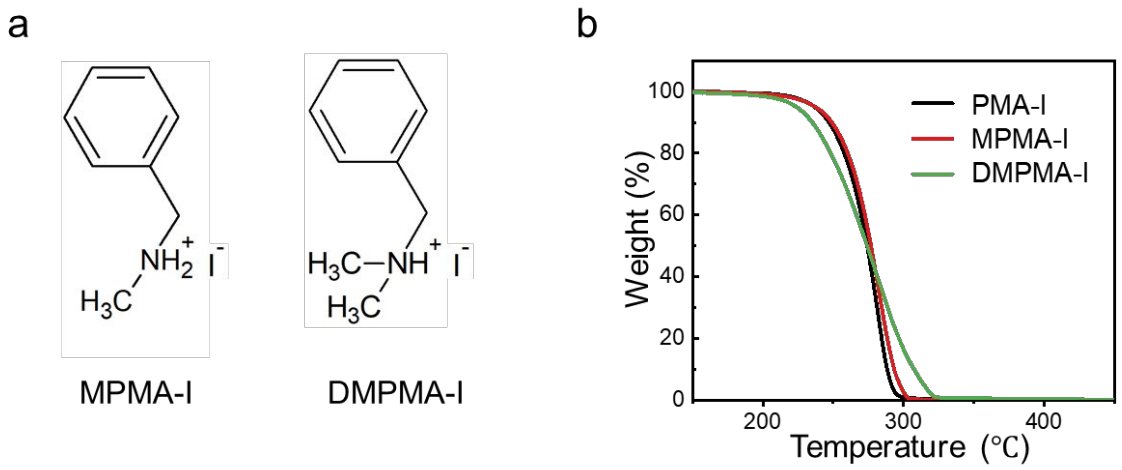

Figure S3. (a) Molecule structure of MPMA-I and DMPMA-I. (b) TGA heating curves of passivation molecules.

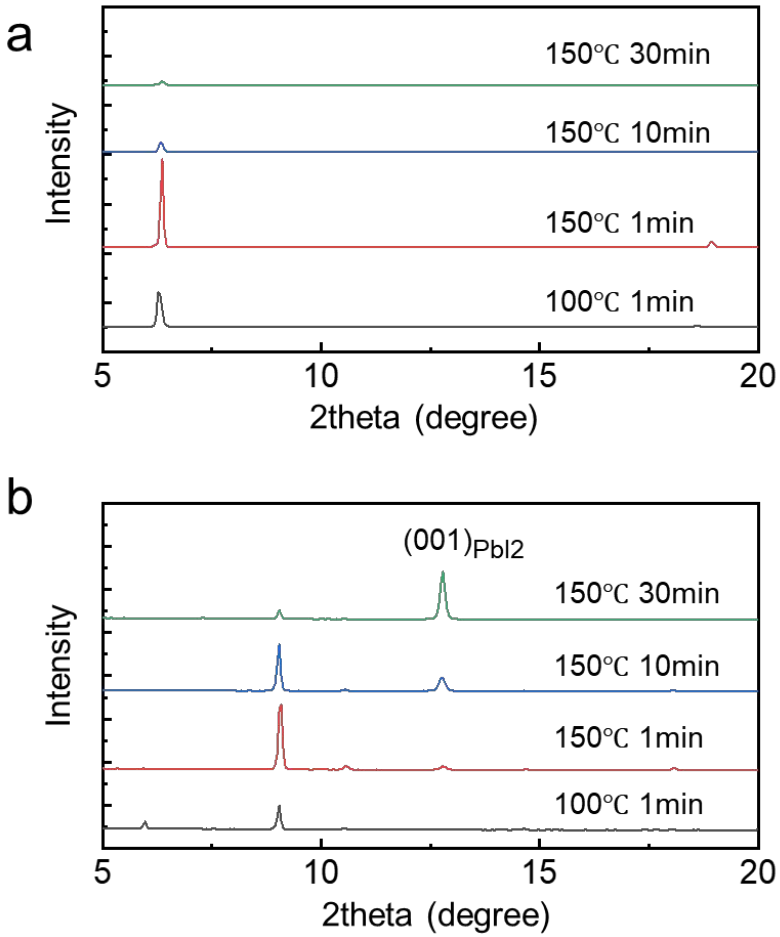

Figure S4. XRD patterns of (a) $MPMA_2PbI_4$ and (b) $DMPMA_2PbI_4$. Films were exposed to thermal stress in ambient air with relative humidity ranging from 25 to 35%.

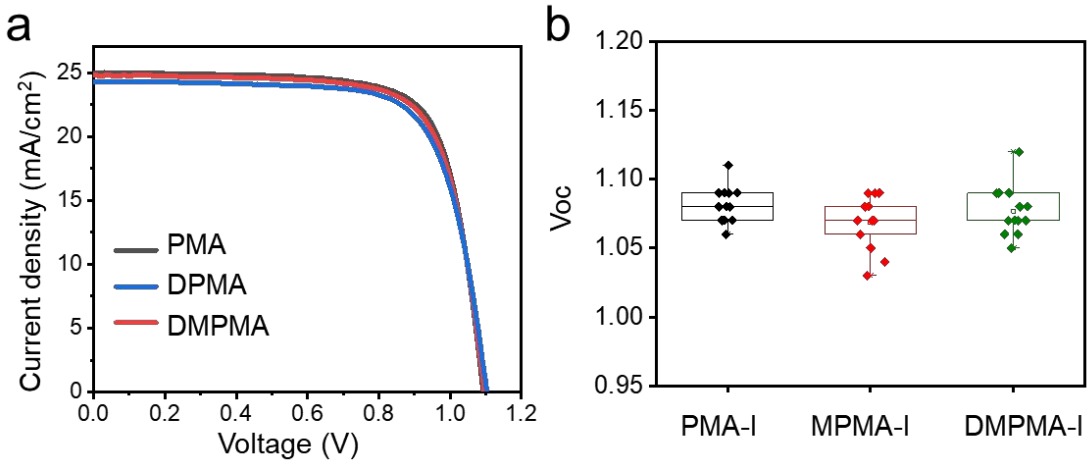

Figure S5. (a) J-V curves of PSCs with 0.5 mol% PMA-I, MPMA-I and DMPMA-I. (b) Histogram of the Voc values.

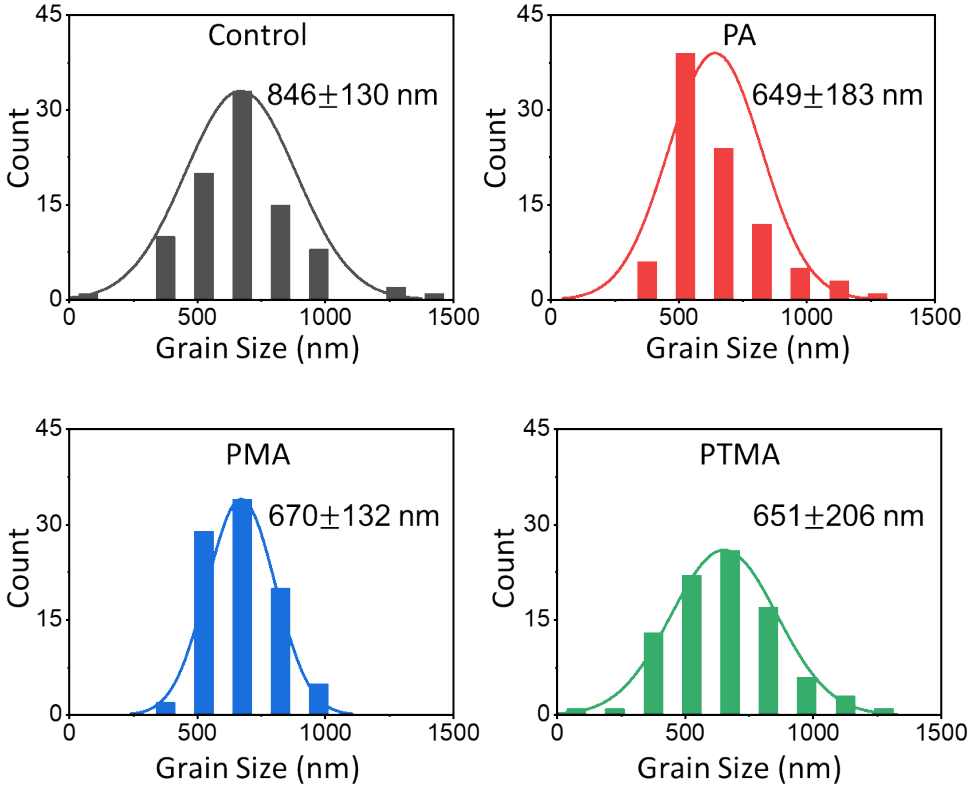

Figure S6. Grain size distribution of perovskite film

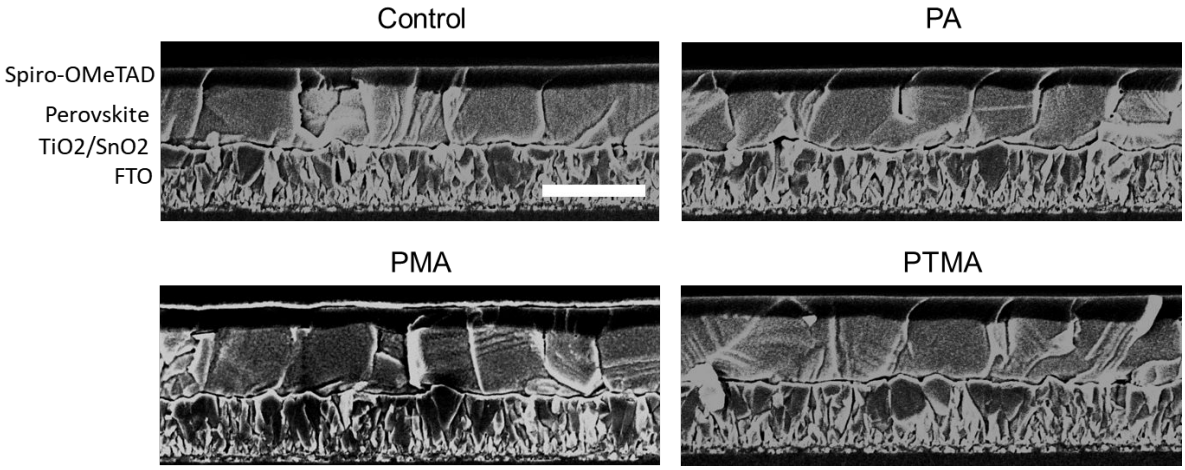

Figure S7. Cross-sectional SEM images of perovskite solar cell (scale bar = 1μm).

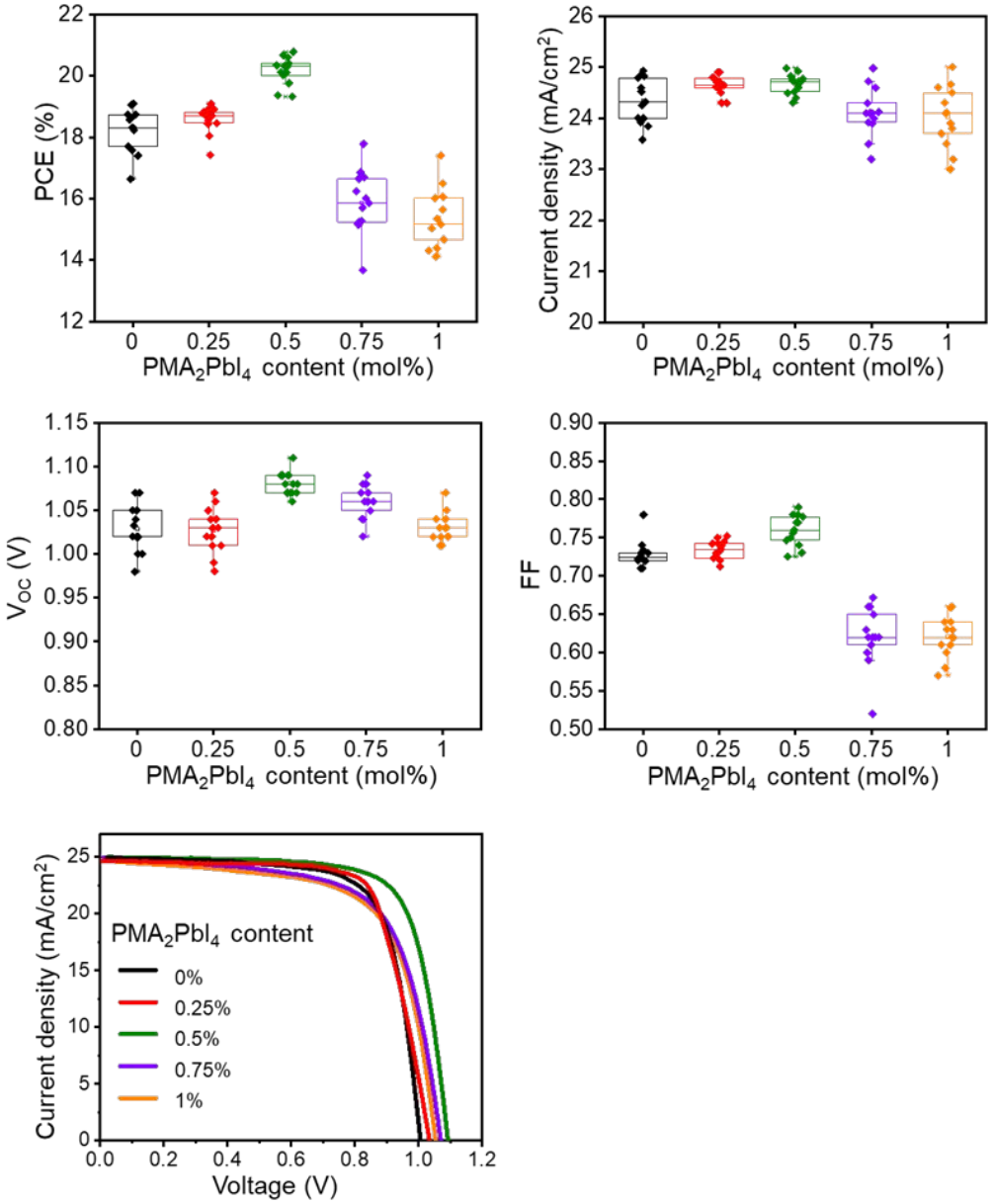

Figure S8. Effect of PMA-I content on photovoltaic parameters. Power conversion efficiency (PCE), fill factor (FF), short-circuit current density (Jsc), and open circuit voltage (Voc) of $(FAPbI_3)_{0.95}(MAPbBr_3)_{0.05}$ with different amounts of added PMA_2PbI_4 perovskite.

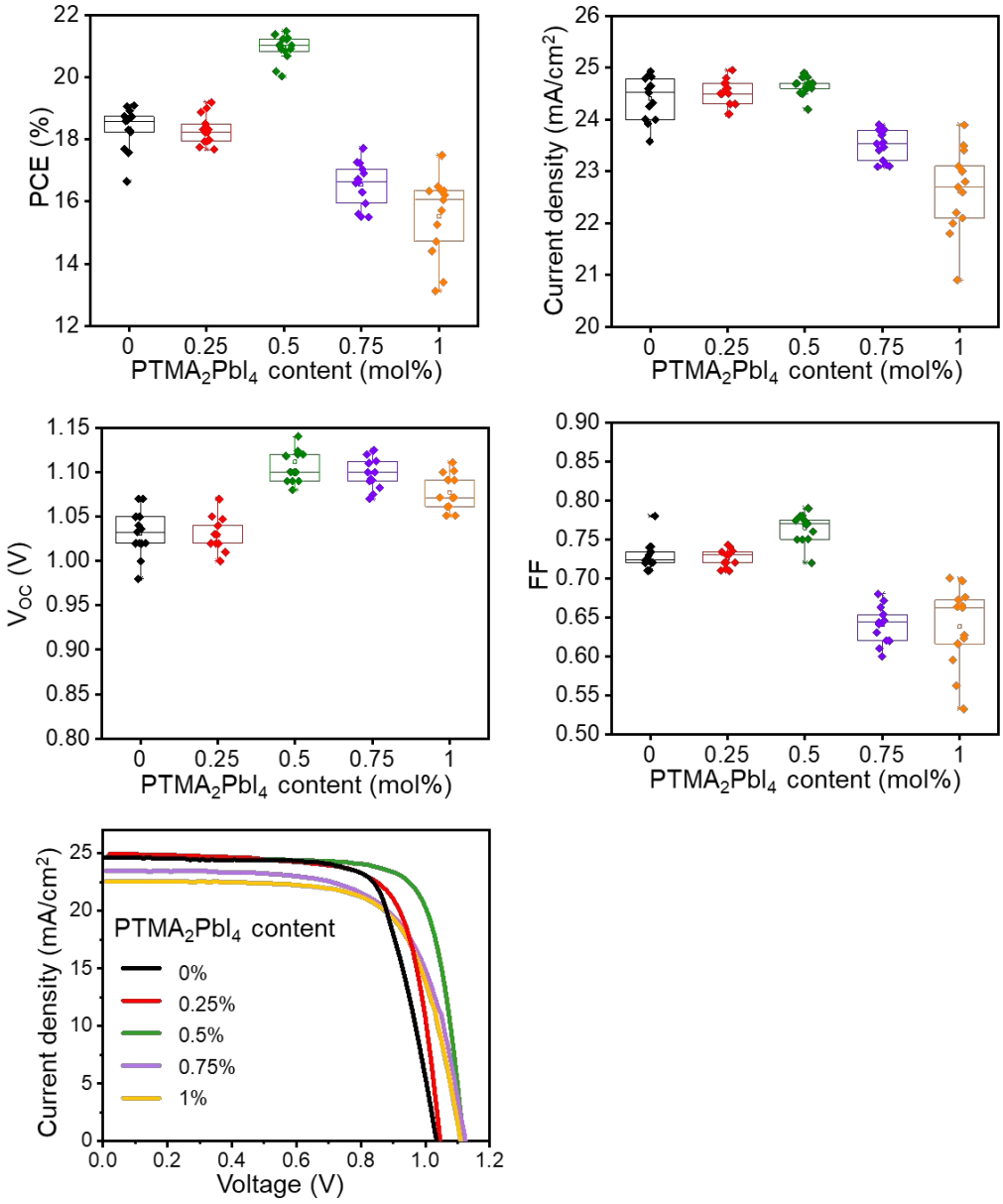

Figure S9. Effect of PTMA-I content on photovoltaic parameters. Power conversion efficiency (PCE), fill factor (FF), short-circuit current density (Jsc), and open circuit voltage (Voc) of $(FAPbI_3)_{0.95}(MAPbBr_3)_{0.05}$ with different amounts of added $PTMA_2PbI_4$ perovskite.

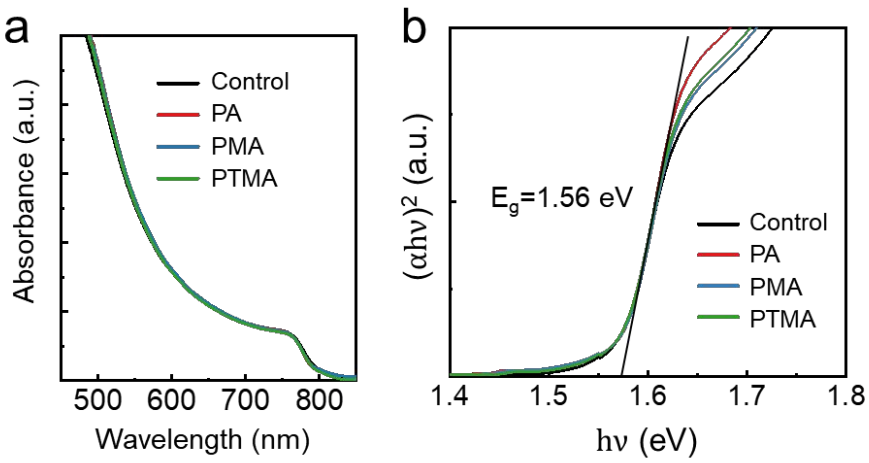

Figure S10. (a) The optical absorption spectra and (b) Tauc plots of perovskite films.

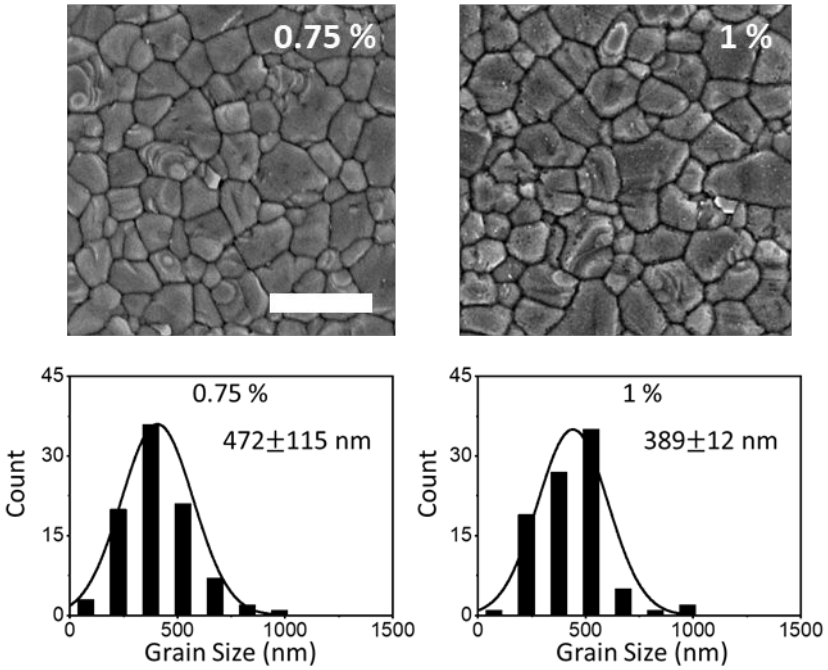

Figure S11. Planar SEM image of perovskite films incorporating 0.75 mol% and 1 mol% PTMA-I (Scale bar = 1μm)

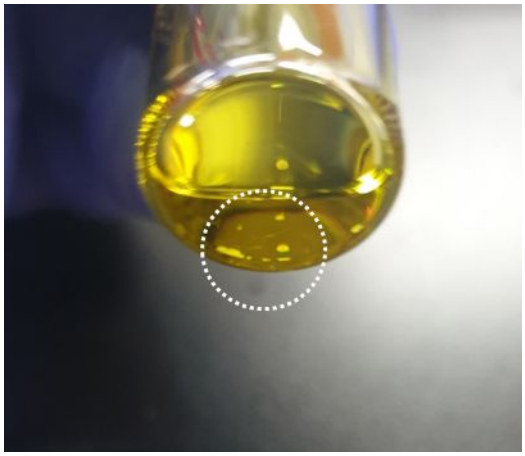

Figure S12. White precipitates start to form when 1 mol% amount of PTMA-I salt is added to the solution. These precipitates are expected to be $PTMA_2PbI_4$.

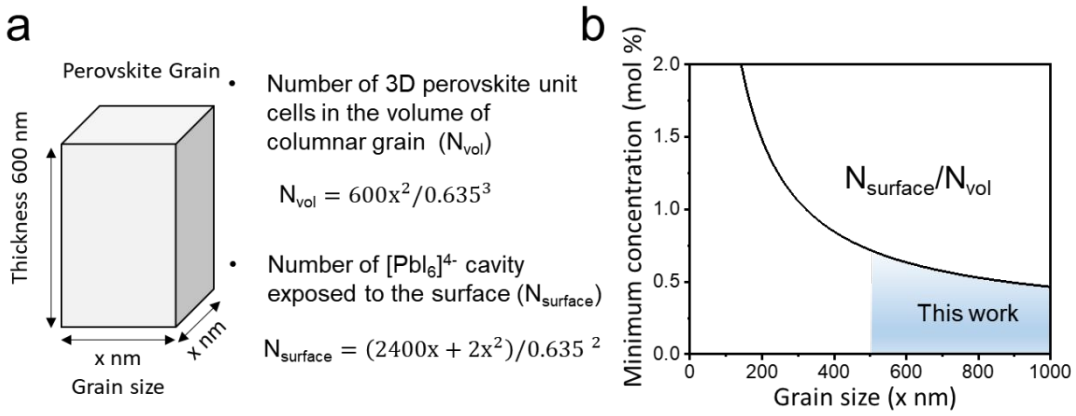

Figure S13. (a) Tetragonal perovskite grain used in the model calculation. (b) Minimum concentration of bulky organic cations required to cover the entire surface of 3D perovskite grain.

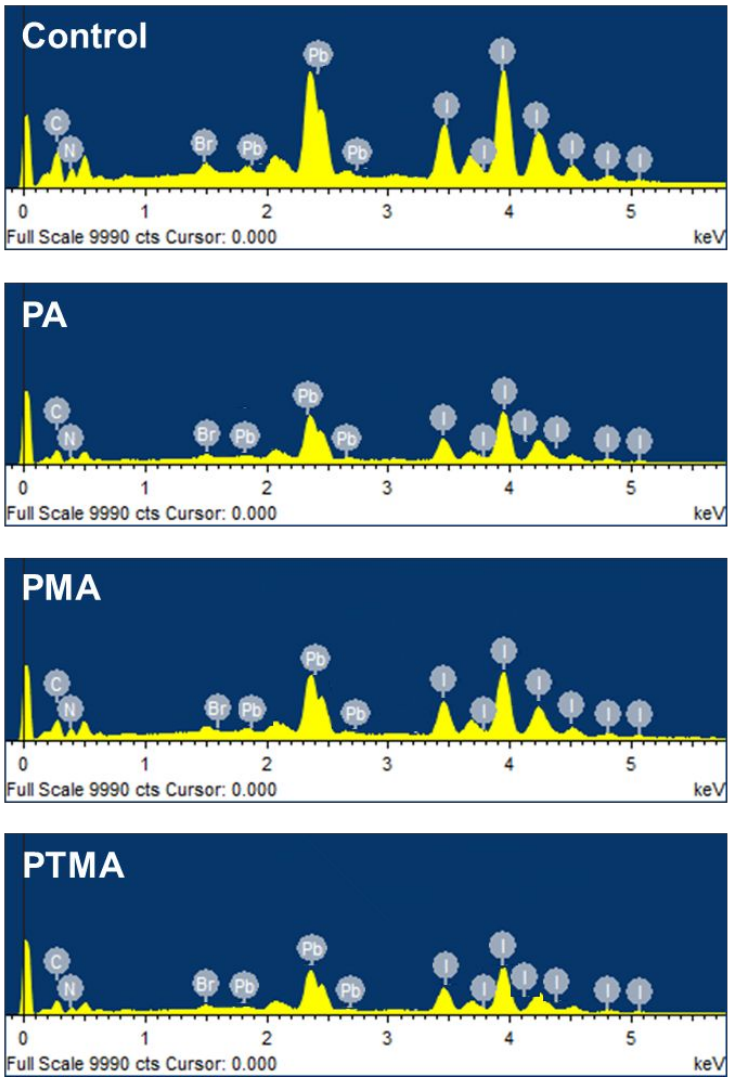

Element	Atomic%
C K	38.58
N K	27.75
Br L	1.3
I L	23.91
Pb M	8.46
Total	100.00

Element	Atomic%
C K	35.93
N K	30.03
Br L	1.33
I L	23.43
Pb M	8.27
Total	100.00

Element	Atomic%
C K	37.27
N K	26.54
Br L	1.34
I L	25.22
Pb M	8.73
Total	100.00

Element	Atomic%
C K	37.11
N K	28.88
Br L	1.37
I L	24.38
Pb M	8.46
Total	100.00

Figure S14. EDS spectra of the perovskite films

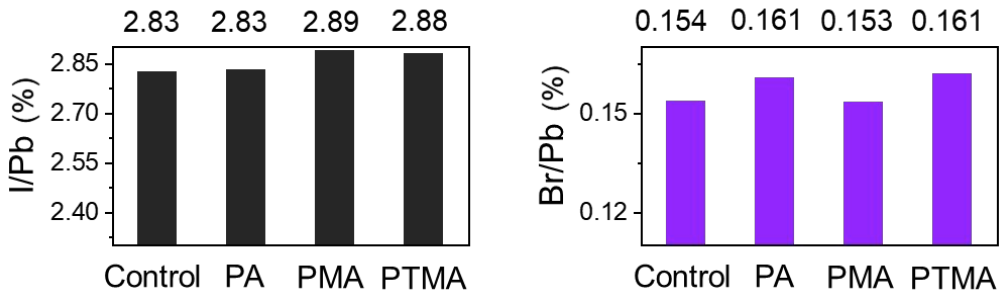

Figure S15. Elemental ratios obtained from the EDS spectrum

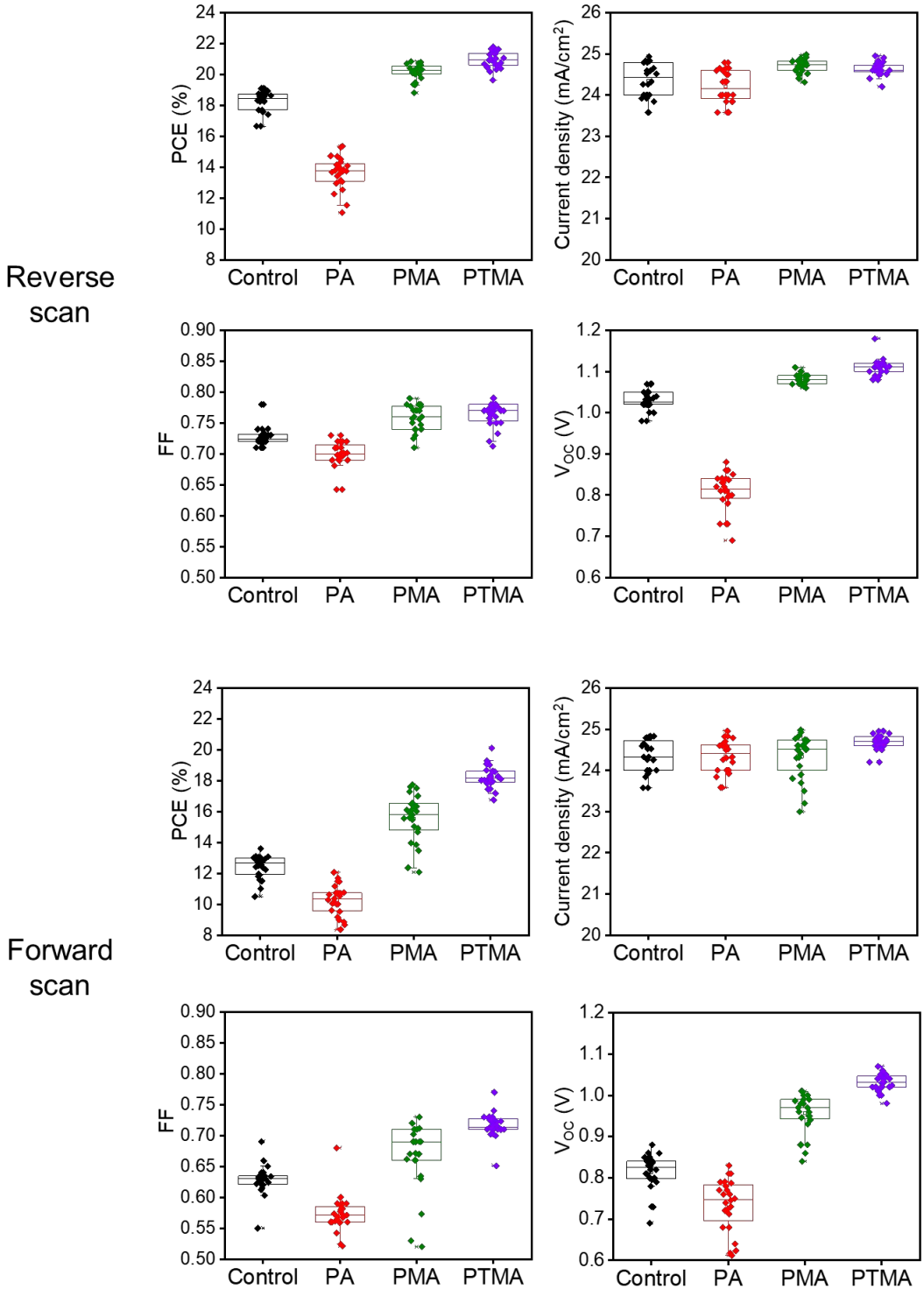

Figure S16. Distribution of photovoltaic performance of PSCs

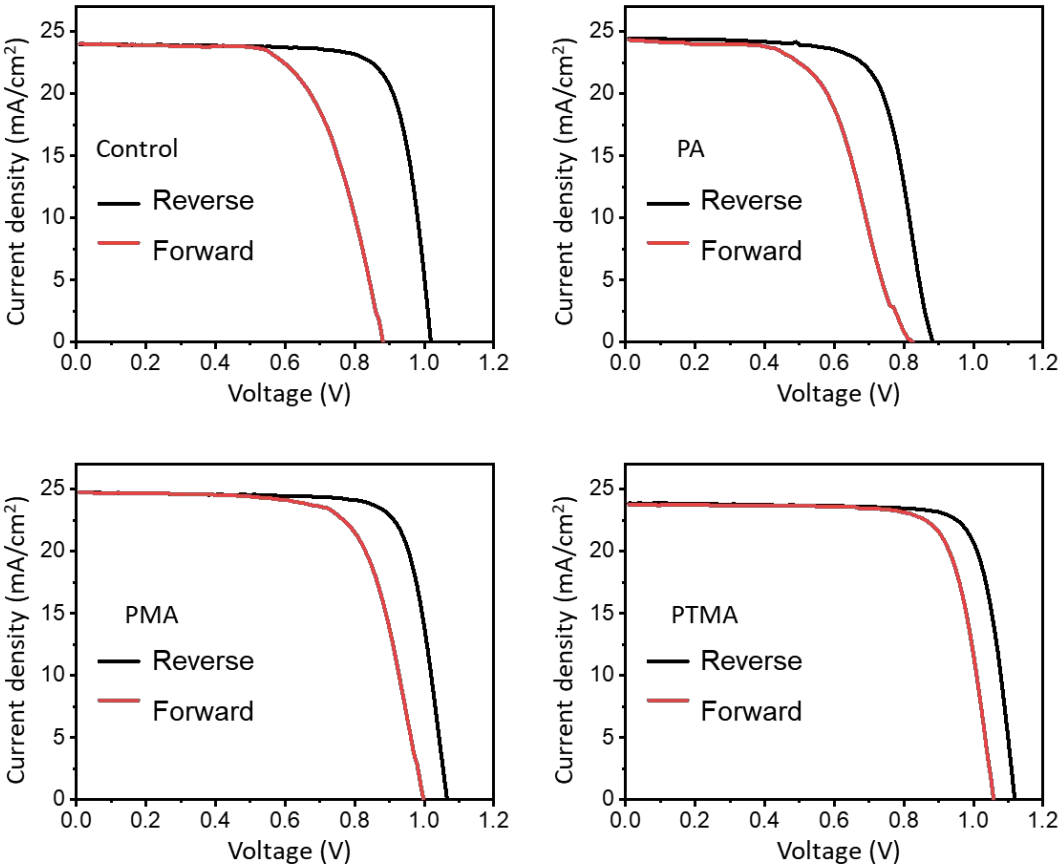

Figure S17. J-V curves of best performing PSCs recorded in both reverse and forward scan directions

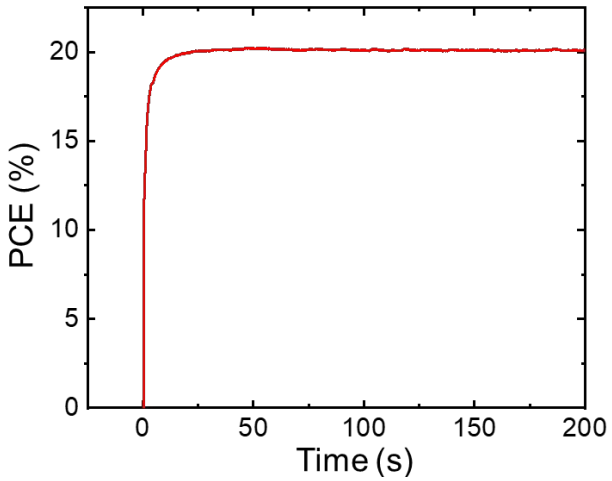

Figure S18. Steady-state PCE measurement of best performing PTMA-I added PSC. The deice was held at constant potential at maximum power point (V_{app}=1 V) to track the stabilized efficiency.

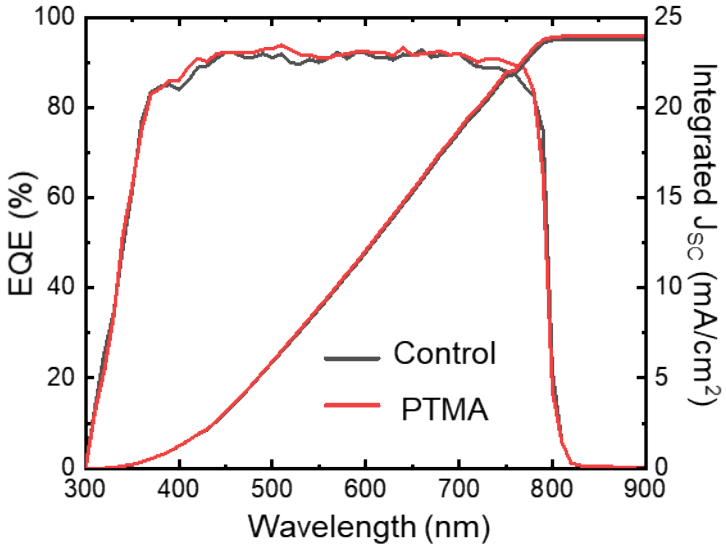

Figure S19. External quantum efficiency plot of PSCs. The integrated current density determined from EQE spectrum is also shown in the right axis.

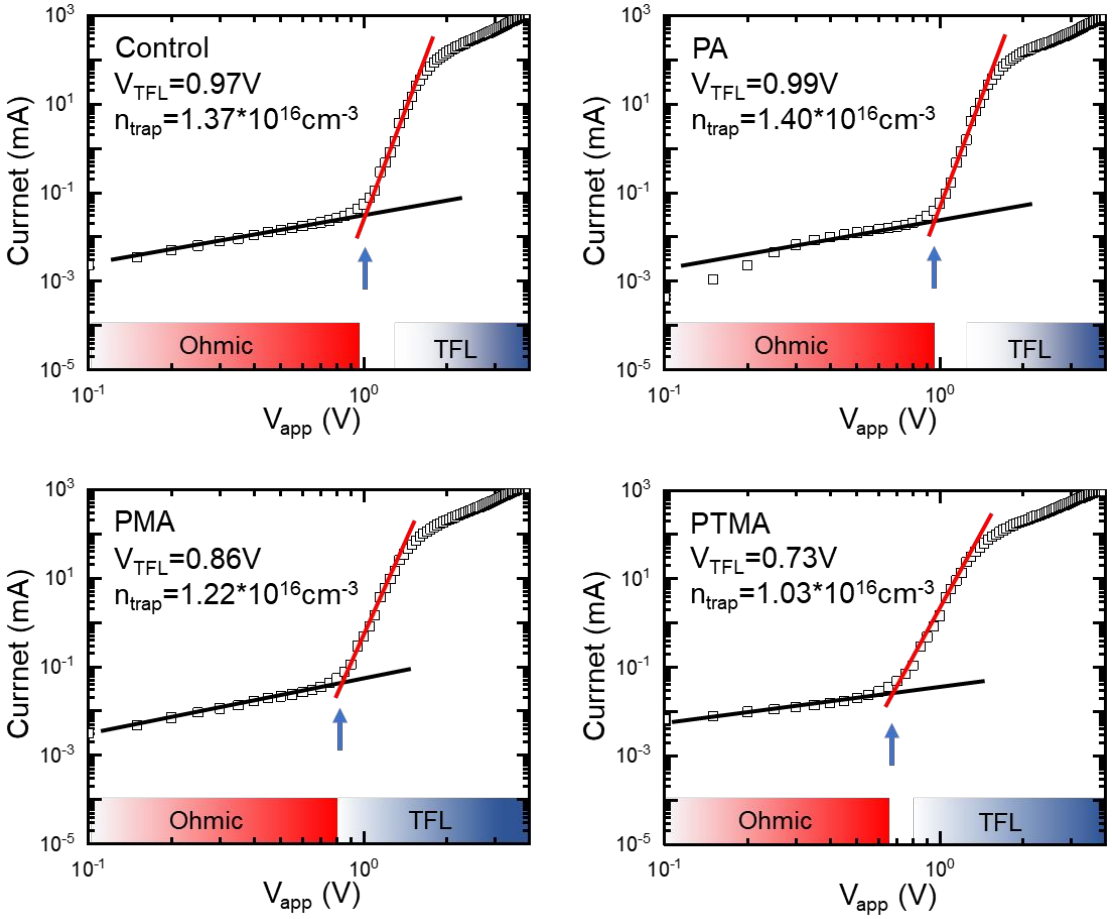

Figure S20. Dark current-voltage curves for electron-only devices, showing ohmic region with n=1 and trap limited region with n>3.

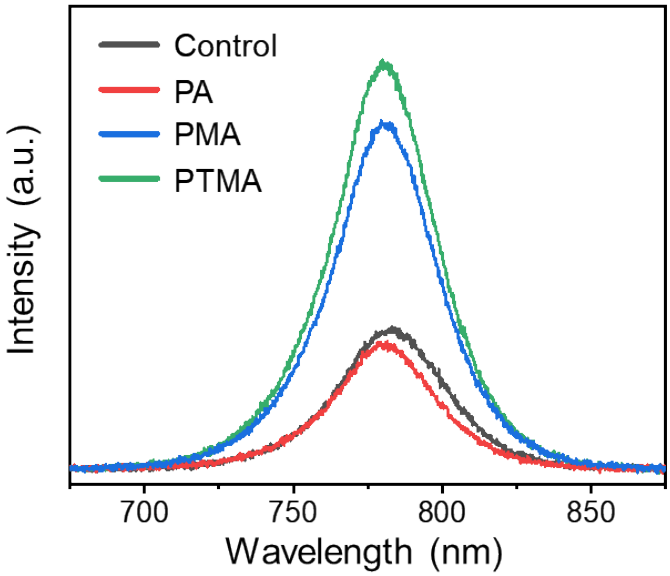

Figure S21. Steady state PL spectra of perovskite layer deposited on glass substrate

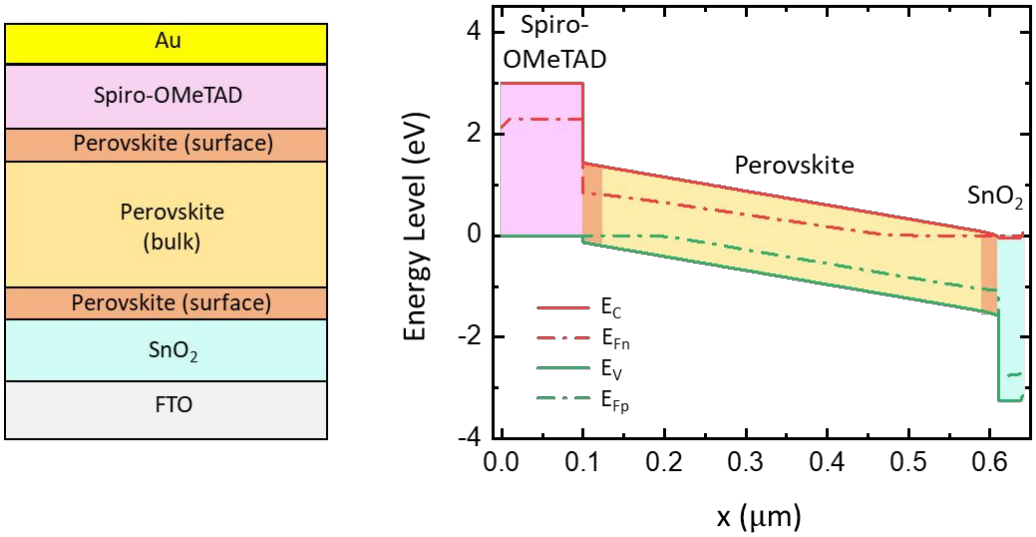

Figure S22. Schematic diagram of device layers defined for SCAPS-1D simulation.

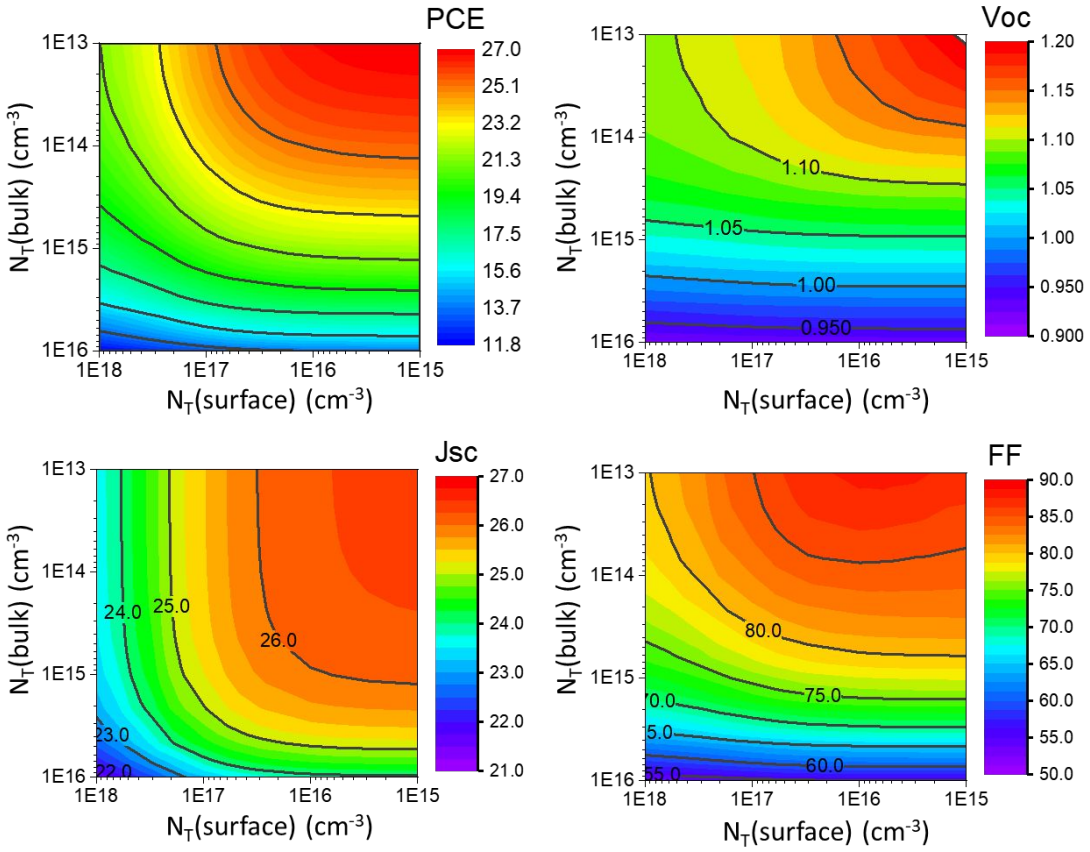

Figure S23. Simulation result of photovoltaic parameters with varying defect densities in perovskite films

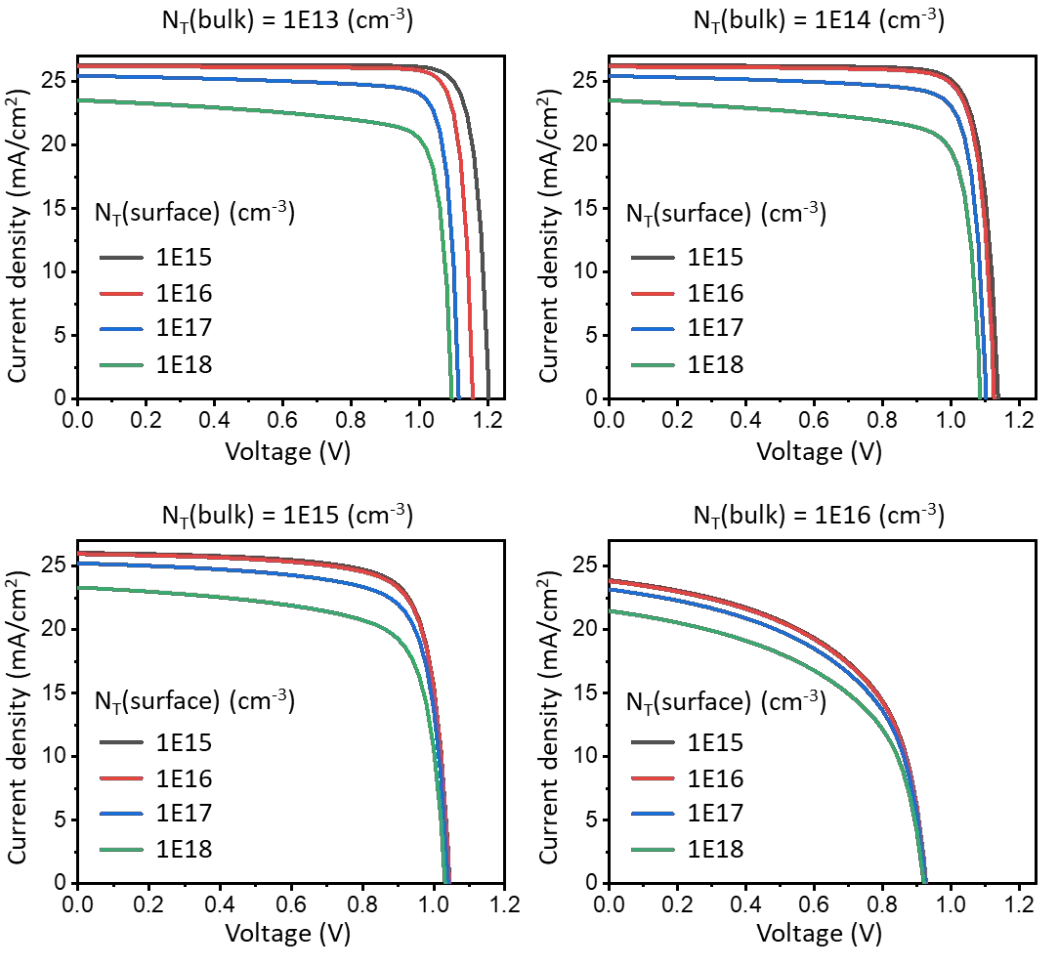

Figure S24. J-V curve of PSCs obtained from drift-diffusion model with varying defect densities

Table S1. Photovoltaic characteristics of the best performing PSC

	Scan direction	V_{oc} [V]	J_{sc} [mA cm^{-2}]	FF	PCE [%]	HI
Control	Reverse	1.02	24.0	0.78	19.1	0.29
	Forward	0.88	24.0	0.64	13.6	
PA	Reverse	0.88	24.5	0.71	15.3	0.24
	Forward	0.83	24.3	0.58	11.7	
PMA	Reverse	1.07	24.8	0.77	20.4	0.17
	Forward	0.99	24.7	0.69	17.0	
PTMA	Reverse	1.11	24.6	0.79	21.6	0.05
	Forward	1.06	24.6	0.77	20.6	

Table S2. SCAPS-1D parameters for the perovskite solar cells

Parameter	ETL (SnO2)	Perovskite bulk	Perovskite surface	HTL (Spiro-OMeTAD)
Thickness (nm)	30	580	10	100
CB/VB effective DOS [cm^{-3}]	1.0 E18 /1.0 E19	1.0 E18/1.0 E19[1]	1.0 E18 /1.0 E19	1.0 E18 /1.0 E19
Acceptor / donor concentration [cm^{-3}]	1.0 E18 /1.0 E19	1.0 E 14 /1.0 E 14[2]	1.0 E 14 /1.0 E 14	1.0 E19 / 1.0 E18
Dielectric constant	9	22	22	3
Electron affinity [eV]	4.0	3.95	3.95	2.4
Band gap [eV]	3.2	1.54	1.54	3
Electron/hole mobility [$cm^2V^{-1}S^{-1}$]	5.0 E-2 / 5.0 E-3	4/4	2/2	5.000E-4 / 5.000E-4
Defect type	Neutral (Gaussian)	Neutral (Gaussian)	Neutral (Gaussian)	Neutral (Gaussian)
Et (eV) / Ech	0.5 / 0.1	0.5 / 0.1[2]	0.5 / 0.1	0.5 / 0.1
Trap density	1.0 E16	1.0 E14 ~ 5.0 E15[3] (variable)	1.0 E15 ~1.0 E20[3] (variable)	1.0 E15
Capture Aross Section for Electrons and Holes (cm^2)	5.0 E-14 / 5.0 E-14	5.0 E-14 / 5.0 E-14[2]	5.0 E-14 / 5.0 E-14	5.0 E-14 / 5.0 E-14

Table S3. Photovoltaic parameters for the simulated J-V curves

N_T(bulk) [cm^{-3}]	N_T(surface) [cm^{-3}]	V_{oc} [V]	J_{sc} [mA cm^{-2}]	FF	PCE [%]
1E13	1E15	1.20	26.3	0.87	27.6
	1E16	1.16	26.2	0.87	26.6
	1E17	1.11	25.5	0.84	24.1
	1E18	1.09	23.6	0.79	20.6
1E14	1E15	1.14	26.3	0.84	25.2
	1E16	1.13	26.2	0.84	24.9
	1E17	1.10	25.4	0.82	23.1
	1E18	1.08	23.5	0.78	19.9
1E15	1E15	1.05	26.1	0.78	21.1
	1E16	1.04	25.9	0.77	21.0
	1E17	1.04	25.2	0.75	19.8
	1E18	1.03	23.3	0.72	17.4
1E16	1E15	0.93	23.9	0.55	12.2
	1E16	0.93	23.8	0.55	12.1
	1E17	0.92	23.2	0.54	11.6
	1E18	0.92	21.5	0.53	10.5

Table S4. Summary of photovoltaic parameters and operational stability of perovskite solar cells reported in literature.

Year	Perovskite	Test condition	Initial PCE (%)	T_{80} (hrs)	Reference
2020	$(FAPbI_3)_{0.95}(MAPbBr_3)_{0.05}$	1 Sun, RT, open-circuit	~21	1163	This work
2018	$GUA_{0.15}MA_{0.85}PbI_3$	1Sun, 60℃, MPP tracking	~18	63	(4)
2017	$Cs_{0.1}FA_{0.74}MA_{0.13}PbI_{2.48}Br_{0.39}$	1 Sun, RT, MPP tracking	~20	450	(5)
2018	$MAPbI_3$	1 Sun, RT, epen-circuit	~19	391	(6)
2019	$MAPbI_3$	1 Sun, RT, MPP tracking	~19	400	(7)
2018	$CS_{0.1}FA_{0.78}MA_{0.12}PbI_{2.55}Br_{0.45}$	1 Sun, RT, MPP tracking	~20	180	(8)
2019	$MAPbI_3$	1 Sun, RT, MPP tracking	~21	810	(9)
2020	$Cs_{0.05}(MA_{0.15}FA_{0.85})_{0.95}Pb(Br_{0.15}I_{0.85})_3$	1 Sun, RT, MPP tracking	~21	1300	(10)
2018	$Cs_{0.05}FA_{0.7}MA_{0.25}PbI_3$	1 Sun, RT, epen-circuit	~20	2400	(11)

Supplementary References

(1) Umari, P.; Mosconi, E.; De Angelis, F. Relativistic GW Calculations on $CH_3NH_3PbI_3$ and $CH_3NH_3SnI_3$ Perovskites for Solar Cell Applications. *Sci. Rep*. **2014**, *4*, article no. 4467, DOI: 10.1038/srep04467.

(2) Khadka, D. B.; Shirai, Y.; Yanagida, M.; Miyano, K. Degradation of Encapsulated Perovskite Solar Cells Driven by Deep Trap States and Interfacial Deterioration. *J. Mater. Chem. C* **2018**, *6* (1), 162-170, DOI: 10.1039/C7TC03733C.

(3) Ni, Z.; Bao, C.; Liu, Y.; Jiang, Q.; Wu, W.-Q.; Chen, S.; Dai, X.; Chen, B.; Hartweg, B.; Yu, Z.; Holman, Z.; Huang, J. Resolving Spatial and Energetic Distributions of Trap States in Metal Halide Perovskite Solar Cells. *Science* **2020**, *367* (6484), 1352-1358, DOI: 10.1126/science.aba0893.

(4) Cho, K. T.; Zhang, Y.; Orlandi, S.; Cavazzini, M.; Zimmermann, I.; Lesch, A.; Tabet, N.; Pozzi, G.; Grancini, G.; Nazeeruddin, M. K. Water-Repellent Low-Dimensional Fluorous Perovskite as Interfacial Coating for 20% Efficient Solar Cells. *Nano Lett*. **2018**, *18* (9), 5467-5474, DOI: 10.1021/acs.nanolett.8b01863.

(5) Jodlowski, A. D.; Roldán-Carmona, C.; Grancini, G.; Salado, M.; Ralaiarisoa, M.; Ahmad, S.; Koch, N.; Camacho, L.; de Miguel, G.; Nazeeruddin, M. K. Large Guanidinium Cation Mixed with Methylammonium in Lead Iodide Perovskites for 19% Efficient Solar Cells. *Nat. Energy* **2017**, *2* (12), 972-979, DOI: 10.1038/s41560-017-0054-3.

(6) Li, X.; Zhang, W.; Wang, Y.-C.; Zhang, W.; Wang, H.-Q.; Fang, J. In-situ Cross-Linking Strategy for Efficient and Operationally Stable Methylammoniun Lead Iodide Solar Cells. *Nat. Commun*. **2018**, *9* (1), article no. 3806, DOI: 10.1038/s41467-018-06204-2.

(7) Han, T.-H.; Lee, J.-W.; Choi, C.; Tan, S.; Lee, C.; Zhao, Y.; Dai, Z.; De Marco, N.; Lee, S.-J.; Bae, S.-H.; Yuan, Y.; Lee, H. M.; Huang, Y.; Yang, Y. Perovskite-Polymer Composite Cross-Linker Approach for Highly-Stable and Efficient Perovskite Solar Cells. *Nat. Commun*. **2019**, *10* (1), article no. 520, DOI: 10.1038/s41467-019-08455-z.

(8) Zhao, Y.; Tan, H.; Yuan, H.; Yang, Z.; Fan, J. Z.; Kim, J.; Voznyy, O.; Gong, X.; Quan, L. N.; Tan, C. S.; Hofkens, J.; Yu, D.; Zhao, Q.; Sargent, E. H. Perovskite Seeding Growth of Formamidinium-Lead-Iodide-Based Perovskites for Efficient and Stable Solar Cells. *Nat. Commun*. **2018**, *9* (1), article no. 1607, DOI: 10.1038/s41467-018-04029-7.

(9) Wang, L.; Zhou, H.; Hu, J.; Huang, B.; Sun, M.; Dong, B.; Zheng, G.; Huang, Y.; Chen, Y.; Li, L.; Xu, Z.; Li, N.; Liu, Z.; Chen, Q.; Sun, L.-D.; Yan, C.-H. A Eu^{3+}-Eu^{2+} Ion Redox Shuttle Imparts Operational Durability to Pb-I Perovskite Solar Cells. *Science* **2019**, *363* (6424), 265-270, DOI: 10.1126/science.aau5701.

(10) Sadegh, F.; Akin, S.; Moghadam, M.; Mirkhani, V.; Ruiz–Preciado, M. A.; Wang, Z.; Tavakoli, M. M.; Graetzel, M.; Hagfeldt, A.; Tress, W. Highly Efficient, Stable and Hysteresis–Less Planar Perovskite Solar Cell Based on Chemical Bath Treated Zn_2SnO_4 Electron Transport Layer. *Nano Energy* **2020**, *75*, article no. 105038, DOI: 10.1016/j.nanoen.2020.105038.

(11) Tsai, H.; Asadpour, R.; Blancon, J.-C.; Stoumpos, C. C.; Durand, O.; Strzalka, J. W.; Chen, B.; Verduzco, R.; Ajayan, P. M.; Tretiak, S.; Even, J.; Alam, M. A.; Kanatzidis, M. G.; Nie, W.; Mohite, A. D. Light-Induced Lattice Expansion Leads to High-Efficiency Perovskite Solar Cells. *Science* **2018**, *360* (6384), 67-70, DOI: 10.1126/science.aap8671.